Supporting Information

Engineering FeS/Fe_3C Nanoparticle Embedded Free-standing Porous Carbon with Numerous Conductive Pathways to Enhance Electron Transfer for Oxygen Electrocatalysis in Rechargeable Zinc-Air Batteries

Siyuan Sun, Fan Yang*, Kexin Wei, Yang Sun, Junpu An, and Yongfeng Li*

State Key Laboratory of Heavy Oil Processing, China University of Petroleum, Beijing, Changping 102249, China

E-mail: yangfan@cup.edu.cn (F. Yang); yfli@cup.edu.cn (Y. Li)

Material characterizations

SEM images were obtained by Hitachisu 8010 operated at 15.0 kV and TEM images were obtained by Tecnai G2 F20 operated at 200.0 kV to investigated the morphology and nanostructure. The corresponding EDS mapping analyses were employed by PV97-61700-ME module and AZtecTEM software. The crystal structure of obtained samples were determined by X-ray diffraction (XRD, Bruker D8 Advance) with a scan rate of 2° min^{-1} (2θ). Graphitization of obtained samples were assessed though Raman spectral by Horibaxploraplus Raman microscopy system under the excitation of 532 nm Ar laser. The specific surface area and pore size were analyzed by N2 adsorption-desorption experiments (SSA4200 Beijing Biaode). The chemical compositions were identified by X-ray photoelectron spectroscopy (XPS, Thermo Scientific Nexsa with Al Kα ray sources). The survey scan was under energy of 100 eV with step size of 1 eV and detailed scan was under energy of 50 eV with step size of 0.1 eV.

Electrochemical measurements

Catalyst ink: All synthesized samples were weighed 5 mg and added into 980 μL water ethanol mixtures (380 μL water and 600 μL ethanol) to disperse by sonication for 15 minutes. And then, 20 μL NafionD-520 solution were dropwise added in above mixtures and further sonicated for 15 min. The ink of commercial Pt/C was prepared in the same way as above method for preparation.

Electrochemical evaluation: The electrochemical properties were evaluated using a CHI760E electrochemical workstation with a rotation control device in a three-electrode cell system. An Ag/AgCl electrode (1M KCl) and a platinum wire were used as reference electrode and counter electrode respectively. The rotating disk electrode (RDE, disk area was 0.1963 cm^2) and rotating ring-disk electrode (RRDE, disk area was 0.2472 cm^2, ring area was 0.186 cm^2) were served as working electrode. The electrolyte was 0.1 M KOH aqueous solution. Cyclic voltammogram (CV) and linear sweep voltammetry (LSV) were carried on from -1.0 to 0.2 V (vs. Ag/AgCl) in O_2/N_2-saturated electrolyte at a scan rate of 0.05 V/s and 0.01 V/s respectively. In RRDE measurements, the constant ring potential was set at 0.314 V (vs. Ag/AgCl) during the

measurements to oxide intermediates of ORR. Electrochemical impedance spectra (EIS) were collected at 0.8 V versus RHE in O_2-saturated electrolyte in the frequency range from 100 k to 0.1 Hz with an amplitude of 5 mV. Relevant calculations and some more detailed test methods were listed in supporting information.

Zinc-air battery measurements

By weighing 3 mg catalyst or Pt/C+RuO_2 dispersing in deionized water containing 500 μl of ethanol and 80 μl of Nafion, respectively, after the mixture was ultrasounded for 30min, apply the prepared slurry onto the carbon cloth to test the performance of zinc-empty battery. The polarization and power density tests of zinc-air batteries were carried out on the CHI 760E electrochemical workstation (CH Instruments, China). Charge/discharge cycling tests were performed on the LAND CT2001 instrument by a 100 s charge step followed by a 100 s discharge step at the same current density of 10 mA cm^{-2}.

DFT Computational details

Based on the density functional theory (DFT), all spin-polarized calculations were performed in CASTEP package. The calculations employed generalized gradient approximation (GGA) and Perdew-Burke-Ernzerhof (PBE) exchange-correlation functional, along with a dispersion correction using the Tkatchenko-Scheffler method. During the geometric optimization, the convergence criteria of energy, force and displacement were set to be 1.0 × 10-5 eV/ atom, 0.01eV/ Å, and 0.001 Å, respectively. To promote the electronic convergence, the Fermi occupation method was applied with a thermal smearing value of 0.25 eV. A 2 × 2 × 1 Monkhorst-Pack grid was used for the Brillouin zone samplings, and the cut-off energy was set as 450 eV. The energy difference tolerance between two steps of a self-consistent field (SCF) process is 2 × 10−6 eV/ atom. A 5 × 5 supercell containing 48 C atoms and 2N atoms was used as the pristine graphene slab, a vacuum slab of 15 Å was added along the surface.

In the ORR reaction, the mechanism in alkaline environment were listed as the following four steps:

$$O2 * + H2O + e - \rightarrow OOH * + OH -$$

$$OOH^* + e^- \rightarrow O^* + OH^-$$

$$O^* + H_2O + e^- \rightarrow OH^* + OH^-$$

$$OH^* + e^- \rightarrow OH^-$$

While in alkaline media, the four-electron reaction steps of OER were described as followings,

$$^* + H_2O \rightarrow OH^* + H^+ + e^-$$

$$OH^* \rightarrow O^* + H^+ + e^-$$

$$O^* + H_2O \rightarrow OOH^* + H^+ + e^-$$

$$OOH^* \rightarrow {}^* + O_2 + e^-$$

The free energy for *OH, *O and *OOH was obtained according to the formula: $\Delta G = U + \Delta EZPE + \Delta E - T\Delta S$, where U stands for applied potential in the calculation, $\Delta EZPE$, ΔE, T, and ΔS are the zero-point energy, the binding energy of the intermediates ($^*OH$, $^*O$, and $^*OOH$), system temperature, and entropy changes, respectively. Moreover, the equilibrium potential is 1.23 eV at room temperature. Therefore, the overpotential of OER is determined by following equations:

$$\eta_{OER} = U_{OER} - 1.23$$

$$U_{OER} = Max(\Delta G_{*OH}, \Delta G_{*O} - \Delta G_{*OH}, \Delta G_{*OOH} - \Delta G_{*O}, 4.92\ eV - \Delta G_{*OOH})/e$$

The overpotential of ORR is expressed as follows:

$$\eta_{ORR} = 1.23 - U_{ORR}$$

$$U_{ORR} = -Max\ (\Delta G_{*OOH} - 4.92\ eV, \Delta G_{*O} - \Delta G_{*OOH,}\ \Delta G_{*OH} - \Delta G_{*O},\ \Delta G_{*OH})/e$$

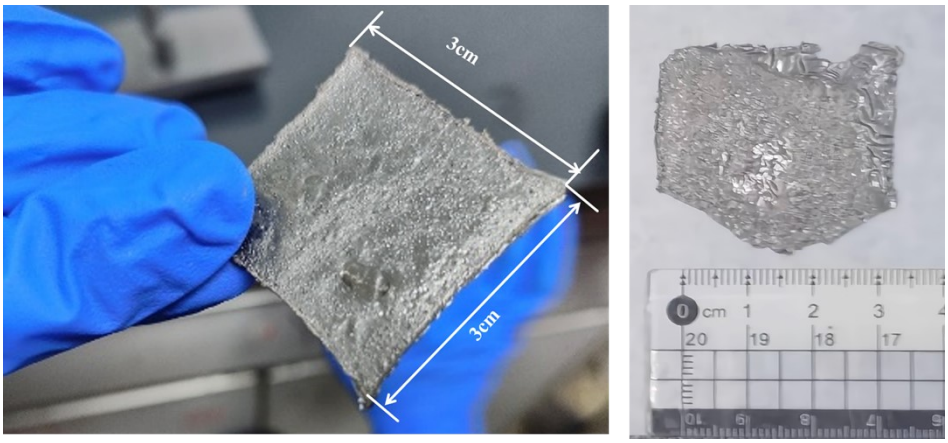

Figure S1. The free-standing carbon-based FeS/Fe_3C@CP sample.

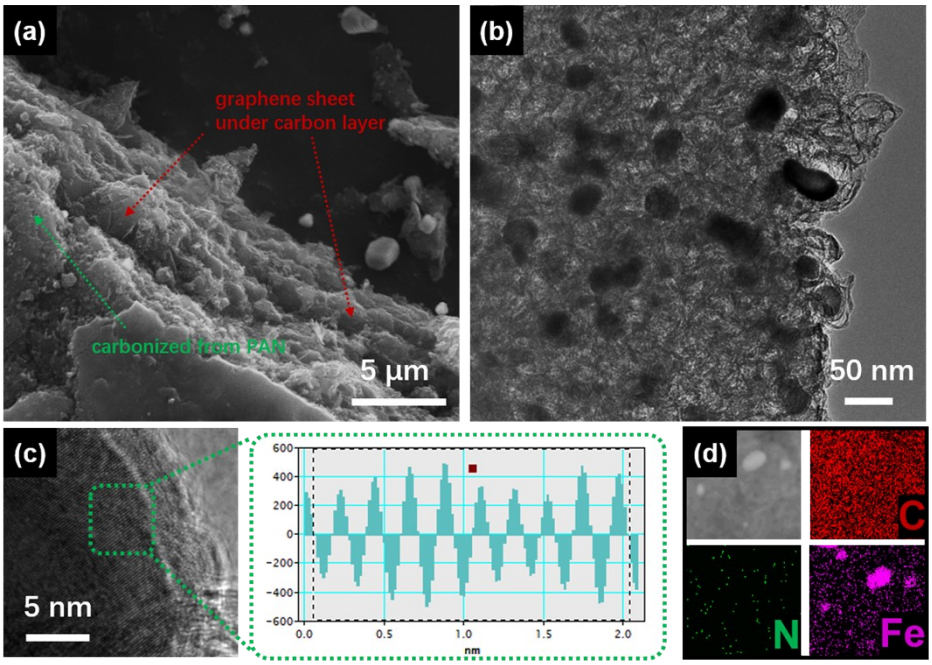

Figure S2. (a) SEM image and (b) TEM image of Fe/Fe_3C@CP. (c) High resolution TEM images and lattice analysis of Fe/Fe_3C@CP. (e) The corresponding EDX mapping patterns of Fe/Fe_3C@CP.

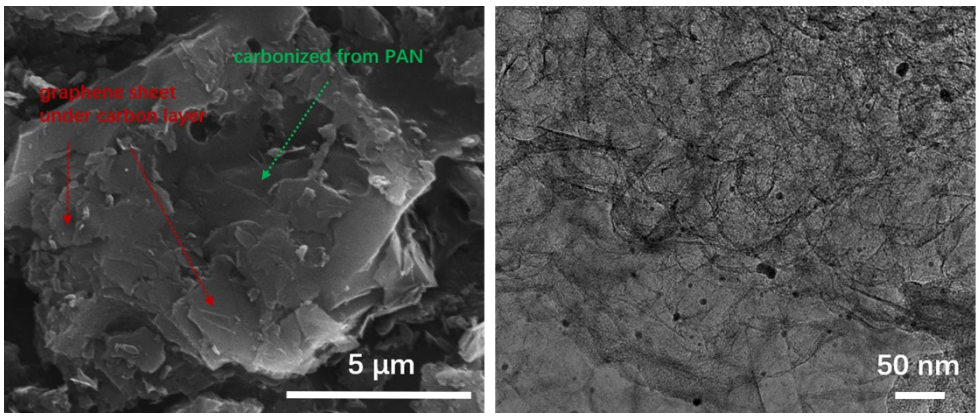

Figure S3. (a) SEM image and (b) TEM image of FeS/Fe_3C@CP-AP.

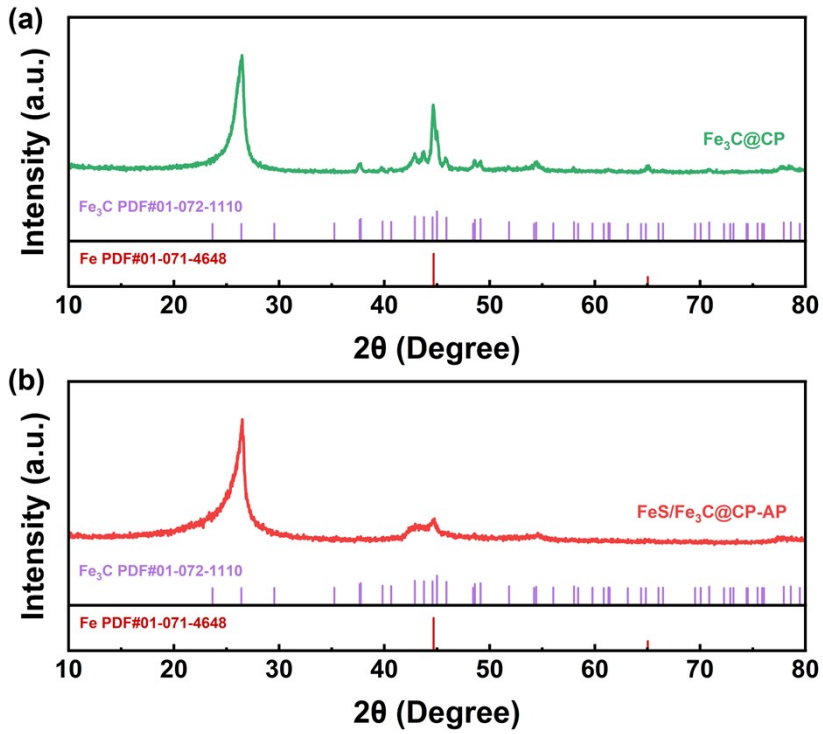

Figure S4. (a) XRD patterns of Fe/Fe_3C@CP and (b) FeS/Fe_3C@CP-AP.

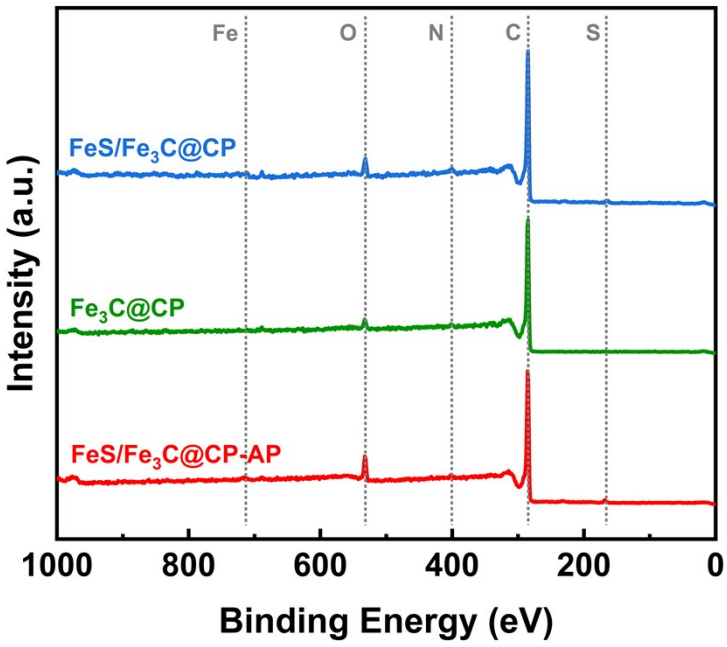

Figure S5. The total XPS spectra of different catalysts.

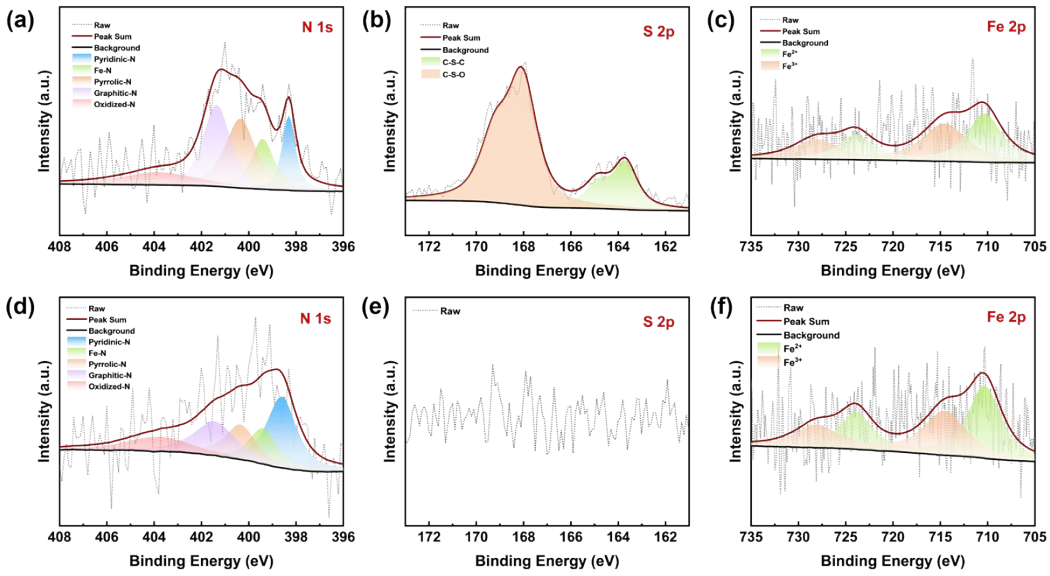

Figure S6. (a-c) N 1s XPS spectra, S 2p XPS spectra, and Fe 2p XPS spectra of FeS/Fe_3C@CP-AP.

(d-f) N 1s XPS spectra, S 2p XPS spectra, and Fe 2p XPS spectra of Fe/Fe_3C@CP.

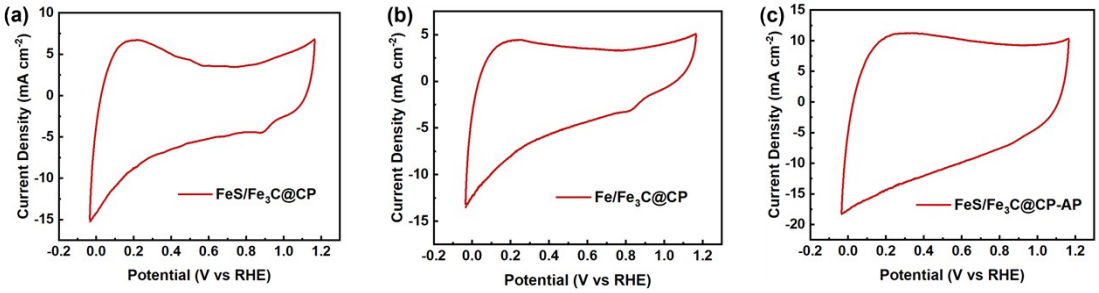

Figure S7. (a-c) ORR CV curves of different catalysts

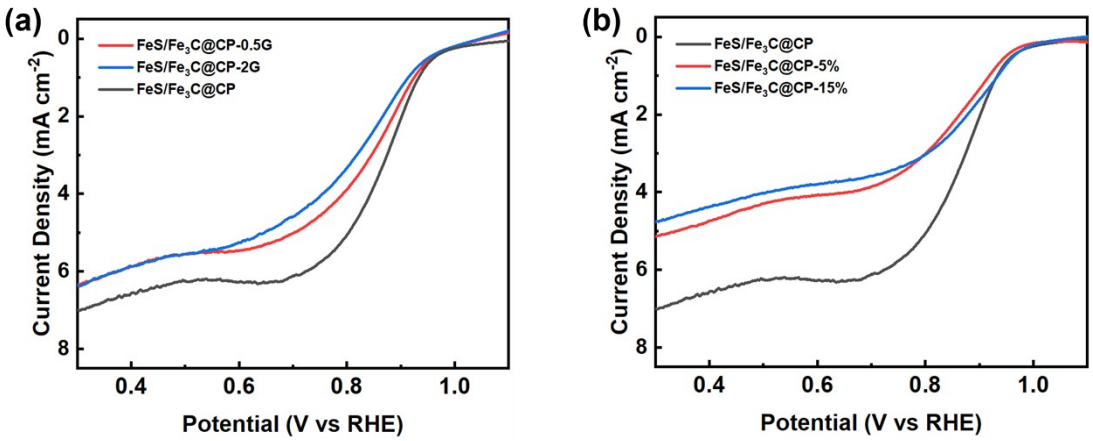

Figure S8. ORR LSV curves of different control samples.

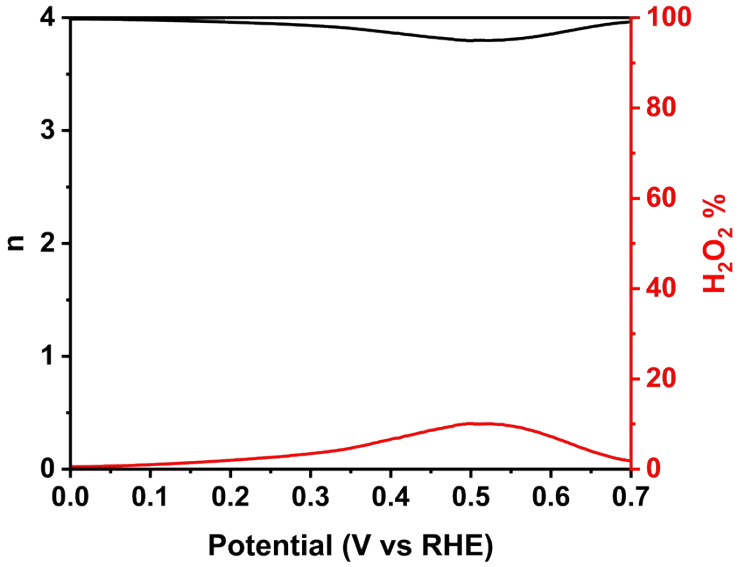

Figure S9. H_2O_2 % and transferred electrons number (n) of FeS/Fe_3C@CP detected by RRDE.

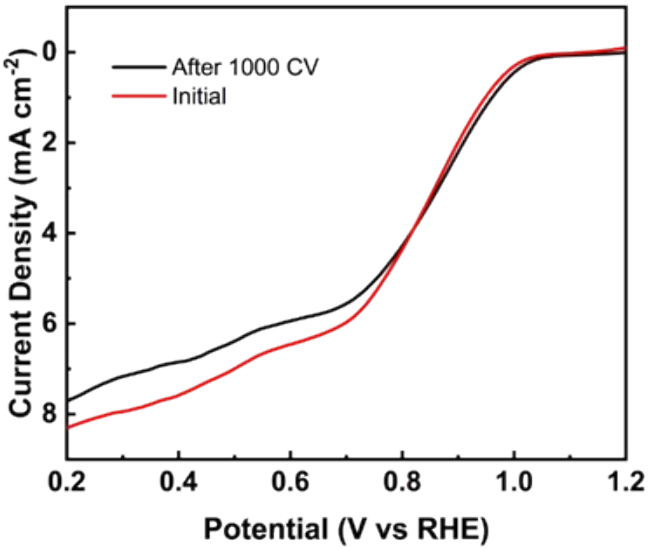

Figure S10. ORR polarization curves of before and after 1000 CV cycles.

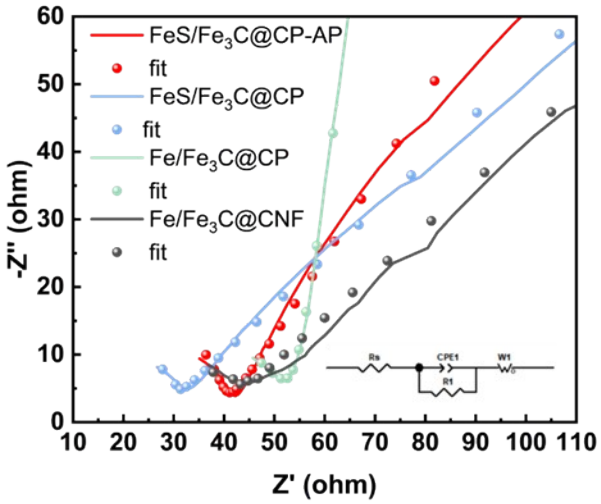

Figure S11. EIS of FeS/Fe₃C@CP, Fe/Fe₃C@CP and FeS/Fe₃C@CP-AP

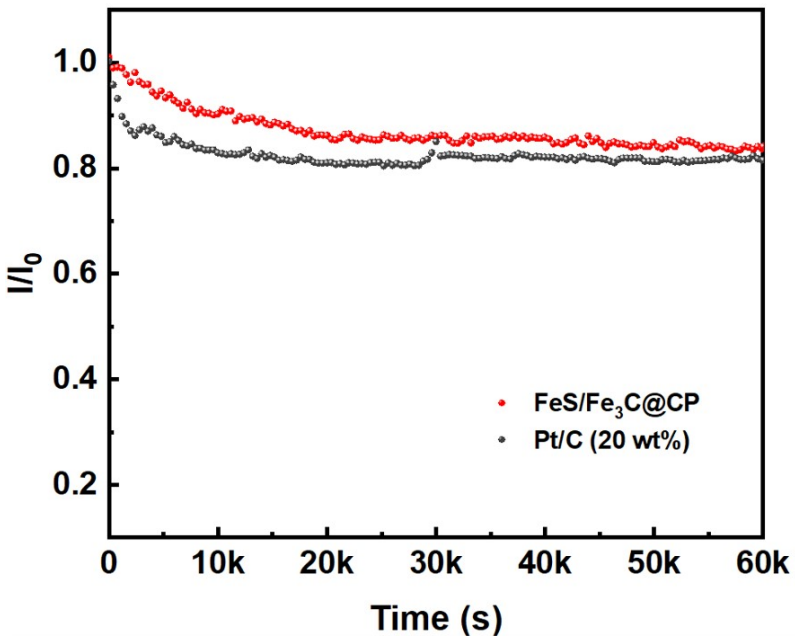

Figure S12. The constant potential test of FeS/Fe_3C@CP and Pt/C.

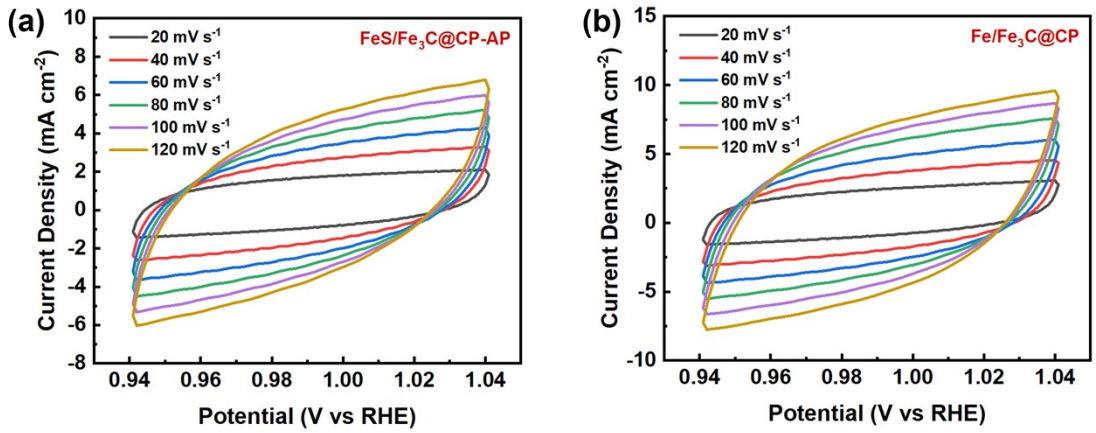

Figure S13. The CV curves of (a) FeS/Fe_3C@CP-AP and (b) Fe/Fe_3C@CP in 1.0 M KOH at different scanning rates.

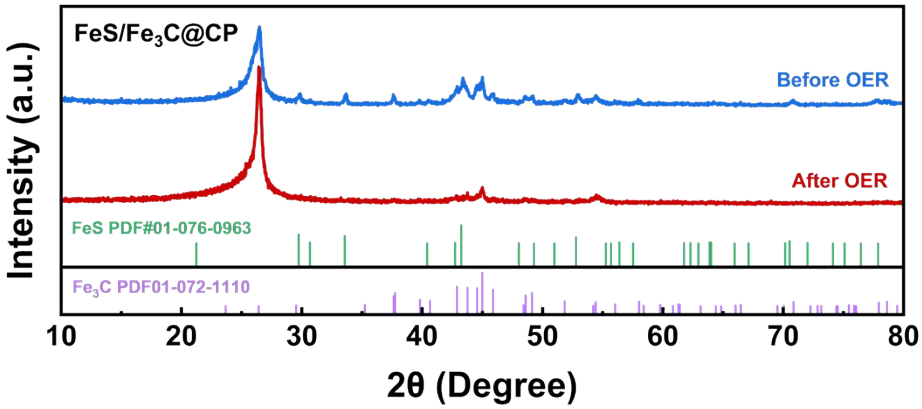

Figure S14. The XRD of FeS/Fe_3C@CP before and after OER constant potential test.

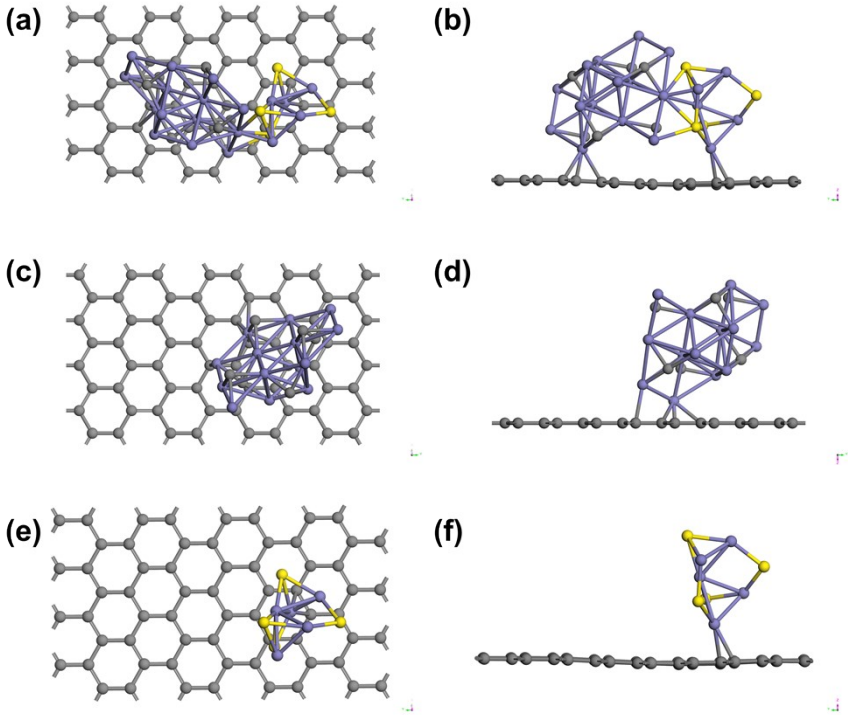

Figure S15. The model of FeS/Fe_3C heterojunction (a, b), Fe_3C (c, d), and FeS (e, f).

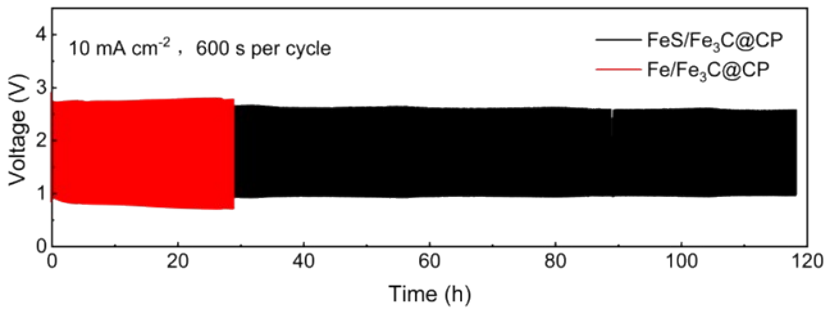

Figure S16. The ZAB test of FeS/Fe_3C@CP and Fe/Fe_3C@CP at 10 mA cm^{-2}

Table S1. A comparison of overall liquid-state ZABs performances among FeS/Fe_3C@CP and reported advanced bifunctional oxygen electrode catalysts.

Sample	Power density (mW cm^{-2})	Charge-discharge durability			Reference
		Current density (mA cm^{-2})	Cycling number	Voltage gap (V)	
FeNi@NCNT-CP	200	10	500	0.99	*Small 2021, 17, 2006183*
FeCo/Se-CNT	173.4	5	210	~0.80	*Nano Lett. 2021, 21, 2255-2264*
Co_p@CoNC	188.8	10	~1080	~0.750	*Energy Storage Mater. 2022, 46, 553-562*
SA&NP-FeCo-NTS	102.2	5	500	0.850	*Adv. Funct. Mater. 2022, 32, 2112805*
Fe-N@Ni-HCFs	172.2	10	600	0.850	*Adv. Funct. Mater. 2022, 32, 2209273*
NiFe-LDH/Fe_1-N-C	205	2	910	0.760	*Adv. Energy Mater. 2023, 13, 2203609*
Fe,Co/DSA-NSC	240	10	600	0.850	*ACS Catal. 2023, 13, 2313-2325*

FeCo-NCNFs-800	74	10	~125	~0.935	*ACS Sustainable Chem. Eng. 2019, 7, 5, 5462-5475*
FeCo@MNC	115	20	114	0.900	*Appl. Catal. B* 2019, *244*. 150-158
FeS/Fe_3C@CP	125	5	~1100	0.91	*This work*